

Article

Hydrogen Reduction in MEP Niobium Studied by Secondary Ion Mass Spectrometry (SIMS)

Tadeusz Hryniewicz ^{1,*}, Piotr Konarski ²  and Ryszard Rokicki ³

¹ Division of BioEngineering and Surface Electrochemistry, Department of Engineering and Informatics Systems, Faculty of Mechanical Engineering; Koszalin University of Technology, Koszalin PL 75-620, Poland

² Vacuum Measurement Laboratory, Institute of Tele- and Radio Technology, Warszawa PL 03-450, Poland; piotr.konarski@itr.org.pl

³ Electrobright, Macungie, PA 18062, USA; ryszardr@ptd.net

* Correspondence: tadeusz.hryniewicz@tu.koszalin.pl; Tel.: +48-94-347-8244

Received: 4 September 2017; Accepted: 10 October 2017; Published: 20 October 2017

Abstract: Niobium, as pure metal and alloying element, is used in a variety of applications, among them in nuclear industries. Niobium is incorporated into nuclear fission reactors due to its enormous strength and low density. Surface finishing of niobium is often performed in electrochemical polishing processes in view of improving its smoothness, corrosion resistance and its surface cleanability. However, the presently used electropolishing process (EP) is intrinsically linked to the subsurface hydrogenation of niobium, which measurably degrades its properties. This is why the annealing operation is used to remove hydrogen from electropolished niobium that is a costly and time-consuming process. The traditional electrolyte consisting of a mixture of 96% H₂SO₄/49% HF acids by volume in a 9:1 ratio has been substituted for the new one, being a mixture of 70% methanesulfonic acid with 49% hydrofluoric acid by volume in a 3:1 ratio. Moreover, the additional imposition of a magnetic field during the electropolishing process (MEP) further increases hydrogen removal, when compared to the hydrogen content achieved by the electropolishing process alone. The aim of the study is to reveal a methodic approach and showing decreasing hydrogenation of niobium samples after consecutive steps of electrochemical polishing. Secondary ion mass spectrometry (SIMS) was used to measure the hydrogen content in the surface layer of as-received AR niobium and in the samples after EP and MEP processes.

Keywords: niobium; magneto-electropolishing (MEP); SIMS; hydrogen content; de-hydrogenation

1. Introduction

Niobium, formerly *columbium*, is a rare, soft, grey and ductile transition metal with the symbol Nb. It is used in a variety of applications, such as superconducting magnets, medical devices, capacitors, optical lenses, barometers, superconducting radio frequency cavities, or electromagnetic radiation detectors, and nuclear industries [1,2]. Moreover, as the alloying element it is used in stainless steels, nickel-, cobalt-, zirconium-, and iron-based super-alloys which are used in aviation industry for jet engines components, rocket sub-assemblies, heat resistant, combustion equipment, etc. [2–4]. Niobium improves the strength of the alloys, especially at low temperatures. It acts as a key element in nuclear fission reactors, due to its enormous strength, low density, high melting point (2477 °C), and low neutron absorption [5].

Niobium is very resistant to corrosion due to a layer of oxide formed on its surface. Although its corrosion resistance is not as outstanding as that of tantalum, the lower price and greater availability make niobium attractive for numerous demanding applications. Niobium forms oxides in the oxidation states +5 (Nb₂O₅), +4, +3, and the rarer oxidation state +2 (NbO). Most common is the pentoxide, precursor to almost all niobium compounds and alloys used in engineering. Pure niobium is used

specifically for superconducting radio frequency (SRF) cavities [6,7], and as niobium-zirconium alloys, for core elements of pressurized water reactors [8,9]. Developed recently, the Zr-Nb alloys provide reliable operation of fuel elements and rod arrays in active reactors and are a basis for new modifications of these alloys created for raising the service properties [8].

Surface finishing of niobium covers both mechanical/abrasive polishing, chemical, and electrochemical polishing processes, with the last also improving surface cleanability. The smoothness and subsurface hydrogen concentration are the most important and often critical factors of the niobium quality. Nowadays, the best method to obtain the smoothest surface of niobium is the electropolishing process. However, the presently used electropolishing process is intrinsically linked to the subsurface hydrogenation of niobium, possibly resulting in the creation of nanohydrides. The annealing operations used to remove hydrogen from electropolished niobium are costly and time-consuming processes. One should mention that the firing of niobium under a vacuum at very high temperature results in a considerable recrystallization [6–9].

Electropolishing processes have been developed for eight decades now to improve surface finishing of metals and alloys [10–24]. Beginning from surface roughness decay and gloss effects appearance, many more interesting features in the metal surface were revealed [25,26], including corrosion resistance and a high improvement of mechanical properties of the treated parts. In recent years, attention was drawn to the problem of hydrogenation of the surface layer after electropolishing. The presently used process for niobium electropolishing is based on the electrolyte consisting of a mixture of 96% H₂SO₄/49% HF acids by volume in a 9:1 ratio. The process gives a satisfactory smooth finish of niobium (average maximum height of the profile Rz in the range of 300 nm), however hydrogenation of subsurface layer [6–8] often appears difficult to avoid. Our earlier studies have shown that by using different electrolytes, which consist of a mixture of 70% methanesulfonic acid with 49% hydrofluoric acid by volume in a 3:1 ratio, the comparable smoothness of niobium surface is obtained [24].

The new electrolyte formula does not introduce hydrogen to the subsurface of an electropolished niobium layer with concentration as the currently used electrolyte does. Additionally, improved surface roughness, by reducing Rz down to below 0.2 μm, was achieved [24] by the imposition of a magnetic field upon the electropolishing process, by the process named magneto-electropolishing MEP [18,19,24,27–34]. The required removal of metal is sped up around 15 times when compared to metal removal by the presently used process [24].

Concerning hydrogen behavior in metals, Pundt and R. Kirchheim [35] provide an interesting insight into metal-hydrogen (M-H) systems. They show that the hydrogen solubility of M-H systems is strongly affected by the morphology and microstructure and the stress between regions of different hydrogen concentration. These problems have been investigated for years now by many researchers, with the obvious conclusion that, in thin films deposited on stiff substrates, compressive stresses evolve during hydrogen loading because the films are effectively clamped to substrates. However, much less attention was directed toward de-hydrogenation of electropolished surfaces, with no extended studies on the effect of magnetic field on M-H system during and after MEP treatment.

Problems associated with hydrogen detection by SIMS are discussed in several papers [36–45], with only two of them [44,45] directed straight at the hydrogenation of metal surfaces after magneto-electropolishing MEP. The main problems found in the literature include: residual gas contamination, primary ion beam contamination and instrumental background. SIMS analysis of hydrogen plays an important role in corrosion studies [40], transistor structure characterization [41], geology studies [42], and hard coating analysis [43].

Electrochemical treatment processes are often characteristic with hydrogenation of metal surface layer. Apart from the electrolyte used, it appears, the additional imposition of a magnetic field during the electropolishing process (MEP) further increases hydrogen removal, when compared to the hydrogen content achieved by the electropolishing process (EP) alone. The aim of the study is to reveal a methodic approach and show decreasing hydrogenation of niobium samples after consecutive

steps of electrochemical polishing. Secondary ion mass spectrometry (SIMS) was used to measure the hydrogen content [44,45] in the surface layer of as-received AR niobium and the samples after EP and MEP processes.

2. Method

2.1. Niobium Samples and Surface Treatment

Samples of dimensions 12 mm × 13 mm (Residual Resistance Ratio 200 (RRR) > 99% pure niobium, WAN CHANG—Albany, OR, USA), cut off from a niobium sheet 3.2 mm thick, were used for the experiments. Three groups of niobium samples were prepared for the studies, two samples in each group. The first two samples, without any further treatment were marked AR—as received, next two were electropolished—marked EP, and two others were magneto-electropolished—marked MEP. The MEP set-up is presented in Figure 1. Niobium sample S as anode A is placed inside the electrolytic cell between two aluminum rods R connected as cathode C. The electrolytic cell with electrolyte E is surrounded by a container with cooling water CW to keep a constant temperature. For magneto-electropolishing MEP, a stack of magnetic rings MS surrounding the system was used (Figure 1).

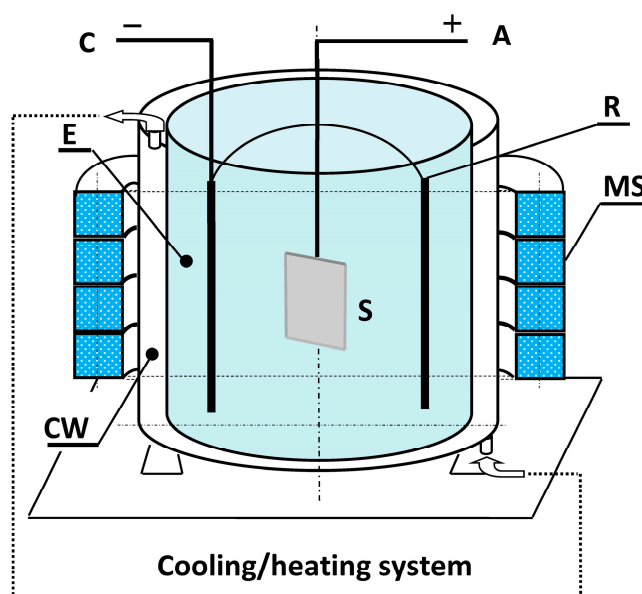


Figure 1. Electropolishing electrolytic cell with superimposed magnetic field: A—anode, C—cathode, MS—stack of ring magnets, CW—cooling water, E—electrolyte, R—aluminum rod, S—niobium sample.

The electropolishing processes, EP and MEP, were performed for two hours in stagnant electrolyte mixture of 70% methanesulfonic acid ($\text{CH}_3\text{SO}_3\text{H}$) and 49% hydrofluoric acid (HF) by volume in 3:1 volume ratio. They were carried out in potentiostatic conditions of 5 V in constant temperature of 25 °C. The magneto-electropolishing MEP was performed in the same electrolyte under the same voltage, temperature, and time. The magnetic field ≈ 100 mT was superimposed on the electropolishing process by using four ring ceramic (ferrite) magnets stacked together: the electrolytic cell was positioned inside ring magnets [27,33].

2.2. Hydrogen Content Measurement

The niobium samples, both as received AR, electropolished EP, and magneto-electropolished MEP, were used to perform measurements of hydrogen content in the surface layer before electrochemical surface treatment, and after these processes. The hydrogen secondary ion currents versus depth profiles were measured on a SAJW-02 analyzer, designed and built in the Institute of Vacuum

Technology (IVT), Warsaw, Poland, equipped with a 06-350E ion gun Physical Electronics (Chanhasen, MN, USA), and 16 mm QMA-410 Balzers quadrupole mass spectrometer (Balzers, Liechtenstein). The ultra-high vacuum system, sample manipulator and load/lock system were done in IVT, Warsaw, Poland. This SIMS system was described elsewhere [36]. 5 keV Ar⁺ primary ion beam was digitally scanned over 3.5 mm × 3.5 mm area while the emission of secondary ions was measured from 1.35 mm × 1.35 mm area. Niobium sputtering rate 0.016 nm·s⁻¹ was calculated basing on Tencor α -step 100 stylus profilometry measurements of much smaller craters (1.2 mm × 1.2 mm) eroded with the same ion beam.

In the SIMS measurements, spectrograms of both the secondary positive and negative ions were registered during Nb samples surface bombardment with Ar⁺ ions. For the depth profile analysis, the following secondary ions were chosen: ¹H⁺, ¹⁶O⁺, ⁹³Nb⁺ and ¹H⁻, ¹⁶O⁻, ⁹³Nb⁻. SIMS studies were performed by using parameters presented in Table 1.

Table 1. Parameters used in the Secondary Ion Mass Spectrometry (SIMS) studies.

Series	Mass Spectrograms	Secondary Ions Selected for the Studies	Scanning Area	Ion Beam Parameters
Primary	0–140 D (+) 0–200 D (–)	-	-	5 keV, Ar ⁺
I	-	¹ H ⁺ (1.27), ¹⁶ O ⁺ , ⁹³ Nb ⁺ and ¹ H ⁻ (1.38), ¹⁶ O ⁻ , ⁹³ Nb ⁻	2 mm × 2 mm	5 keV, Ar ⁺
II	-	H ⁺ (1.41), H ₂ ⁺ , O ⁺ , ⁹³ Nb ⁺	1 mm × 1 mm	5 keV, Ar ⁺
III	-	H ⁺ (1.41), H ₂ ⁺ , O ⁺ , ⁹³ Nb ⁺	3.5 mm × 3.5 mm	5 keV, Ar ⁺

3. Results

3.1. First Series of Experiments

The registered mass spectrograms are given in Figure 2. Spectrograms of the secondary positive ion mass are presented in Figure 2a, and negative ion mass in Figure 2b. Results displayed in Figure 2 show that the AR sample surface is much more contaminated by foreign particles than those two other Nb samples, after EP and MEP. Higher are currents of the positive ions of Na⁺, K⁺ and O⁺. In case of the analysis of negative ions, one can also note that higher are currents of ions of C⁻, O⁻, F⁻ and Cl⁻.

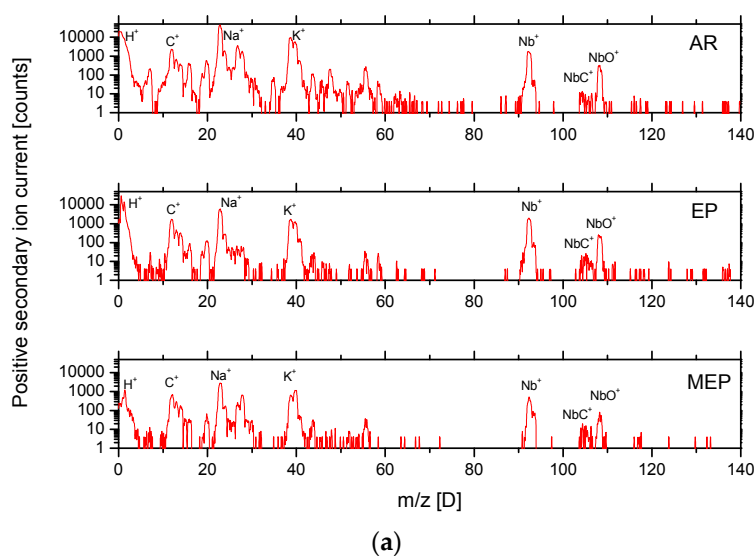


Figure 2. Cont.

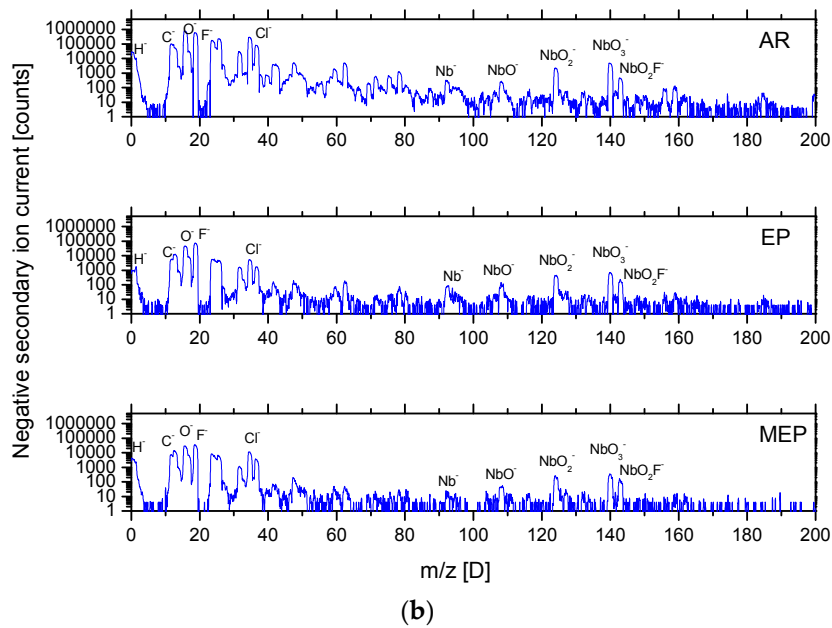


Figure 2. Mass spectrograms of positive (a) and negative (b) secondary ion currents. Results taken of three niobium samples: AR, EP, and MEP are presented.

Results presented in Figure 3 confirm that the near-surface layer of the AR sample is more contaminated in comparison with those of the EP and MEP samples. It is also apparent that currents of the secondary ions of hydrogen and oxygen in MEP sample are higher in comparison with currents measured on EP niobium sample. Higher level of O^- ions measured on MEP sample, in comparison with EP sample, is meaningful.

The ion etching area in the first series of SIMS measurements was equal $2\text{ mm} \times 2\text{ mm}$. One can easily conclude that in case of ion etching of the area $2\text{ mm} \times 2\text{ mm}$ with the same ion beam (previous series of results) the rate of ion etching was $0.05\text{ nm}\cdot\text{s}^{-1}$.

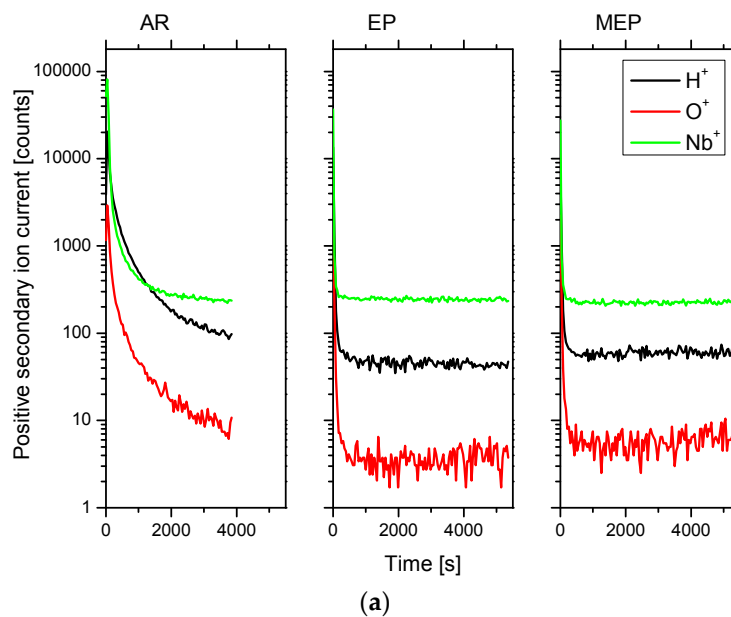


Figure 3. Cont.

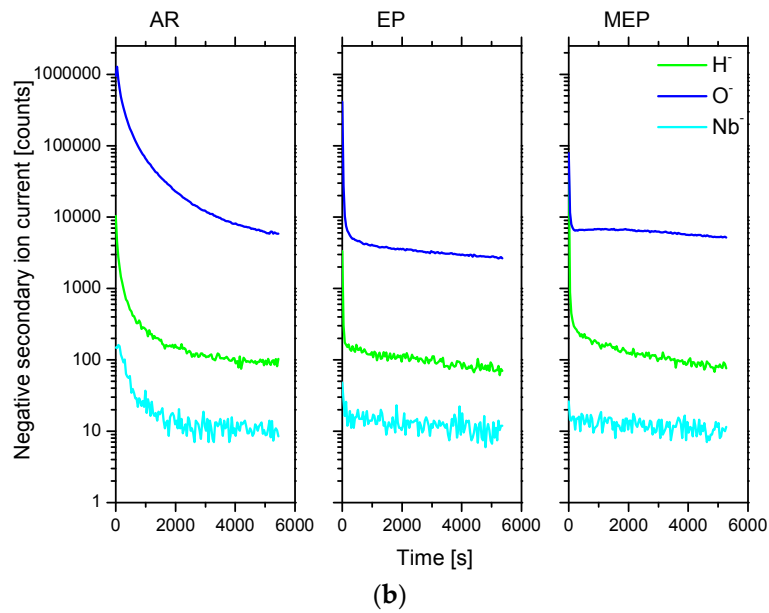


Figure 3. Rough results of SIMS depth analyses for positive (a), and negative (b) ions studies. The values of currents of the secondary ions vs. etching time are presented (at the electron beam of the energy of 5 keV). The ion etching area: 2 × 2 mm, analysis area: 0.8 × 0.8 mm. Three niobium samples were studied: AR, EP, and MEP.

To compare emission of hydrogen ions for the three studied Nb samples, the ratios of these currents and niobium ions currents were calculated. The results are displayed in Figure 4. One may easily notice that the relative emission for hydrogen ions is slightly higher on MEP sample in comparison with that one measured on EP sample.

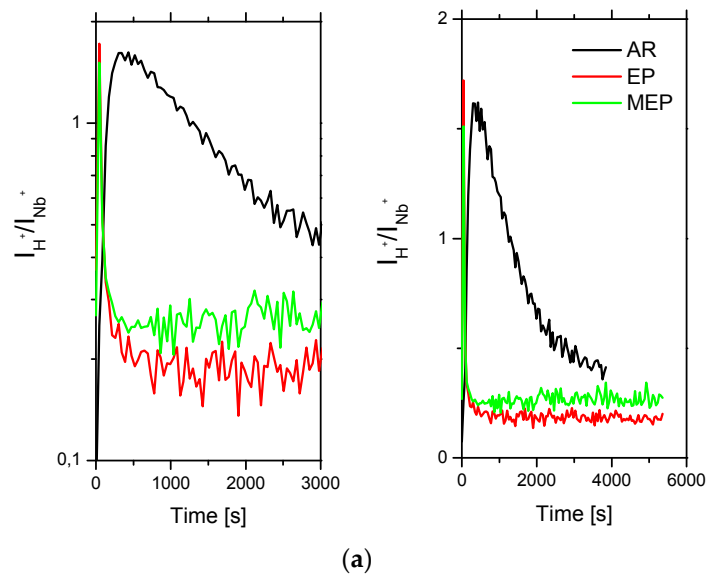


Figure 4. Cont.

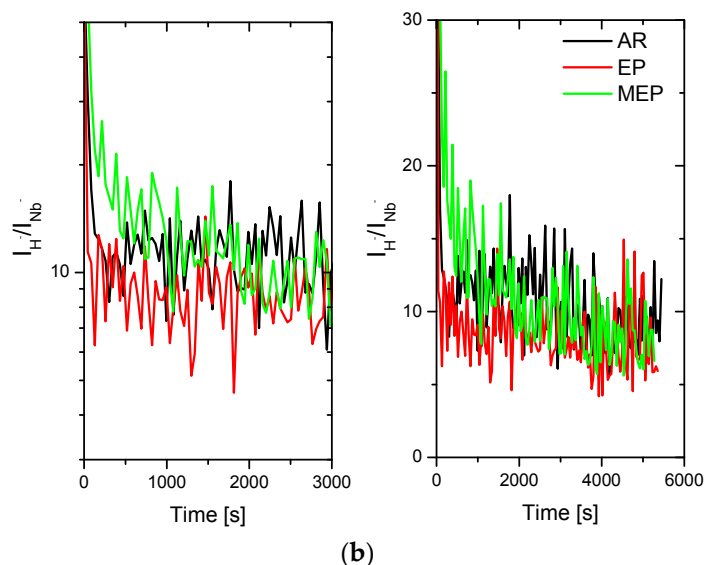


Figure 4. Dependence of ratios of secondary ions current of hydrogen to secondary ions current of niobium on the time of ionic etching. Etching time of 5500 s corresponds with the thickness of niobium etched layer equaling a few hundreds of nanometers; in (a) there are given ratios of positive secondary ions currents, and in (b) ratios of negative secondary ions currents.

Results obtained for positive secondary ions present the difference in the whole range of ion etching. On the other hand, the results obtained for negative secondary ions relate to the depth corresponding with half of the ion etching depth.

3.2. Second Series of Experiments

The second series of SIMS measurements was carried out on two niobium samples, after EP and MEP. Positioning of H^+ and H_2^+ peaks on the mass spectrogram were chosen very carefully. Positive secondary ions with four masses: 1, 2, 16, and 93 were chosen/appointed for the depth profile analysis. Ion etching using beam 5 keV Ar^+ was performed. The area of ion etching was equal $1\text{ mm} \times 1\text{ mm}$. Time of the etching was 5000 s so that obtained crater was 1 micrometer in depth. Therefore, the rate of niobium etching under these conditions of ion etching process was equal $0.2\text{ nm}\cdot\text{s}^{-1}$. In the first series of SIMS measurements, under ionic etching of area $2\text{ mm} \times 2\text{ mm}$ using the same ion beam, the rate of ionic etching was equal $0.05\text{ nm}\cdot\text{s}^{-1}$.

Rough results of SIMS depth analysis obtained in the second series of measurements are given in Figure 5. Changes in the values of ion secondary currents vs. time of etching are apparent, using the etching beam 5 keV. With the assumed area of ion etching $1\text{ mm} \times 1\text{ mm}$, the area of analysis was $0.4\text{ mm} \times 0.4\text{ mm}$. The obtained results show that investigated positive secondary currents are very similar on both samples, EP and MEP.

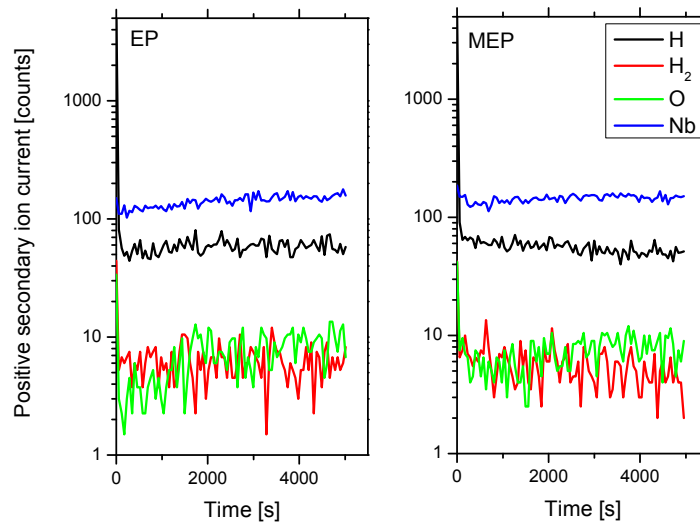


Figure 5. Rough results of SIMS profile analysis obtained in the 2nd series of measurements. The secondary ion currents are displayed. Surface area of ion etching: 1 mm × 1 mm, analysis area: 0.4 mm × 0.4 mm, two Nb samples were used for the study: EP—on the left, and MEP—on the right.

In Figure 6, the ratios of secondary ion currents for positive hydrogen (H^+ and H_2^+) to secondary ion currents of niobium on time (a) and depth (b) of the ion etching are given, related to EP and MEP niobium samples. Time of ion etching was 5000 s (Figure 6a), with the depth of etched niobium layer equal to 1 micrometer (Figure 6b).

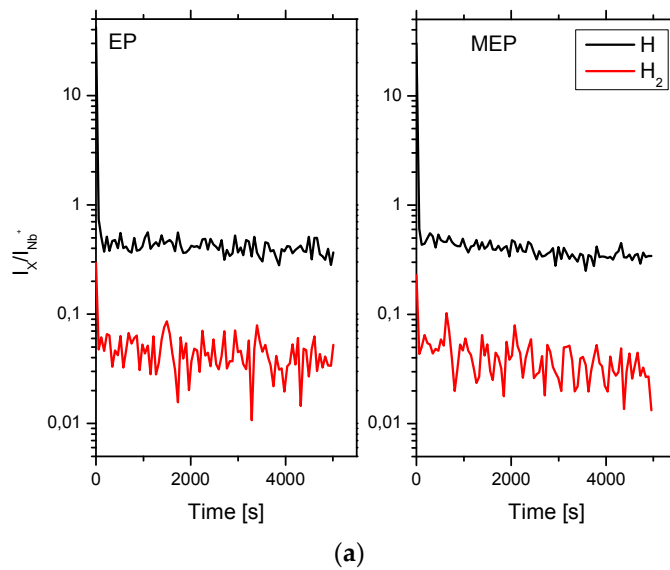


Figure 6. Cont.

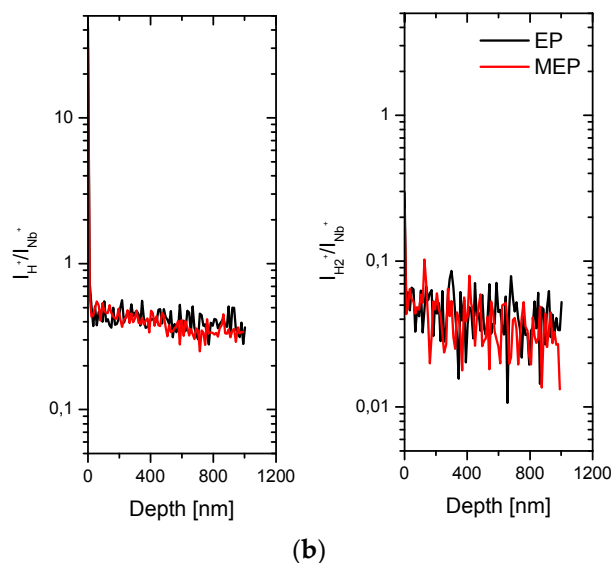


Figure 6. Dependence of ratio of secondary ion currents for positive hydrogen (H^+ and H_2^+) to secondary ion currents of niobium on time of the ion etching. Time of ion etching: 5000 s (a), the depth of etched niobium layer equals to 1 micrometer (b).

In Figure 7, the results of the ratios of secondary ion currents for positive hydrogen (H^+ and H_2^+) to secondary ion currents of niobium on depth of the ion etching are given, also related to EP and MEP samples. Here the values of ordinates are presented in a smoothed form.

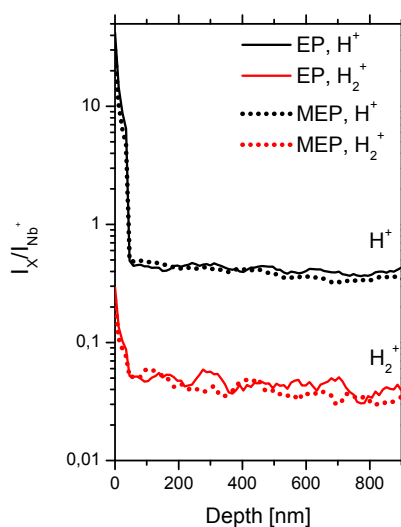


Figure 7. Dependence of ratio of secondary ion currents for positive hydrogen (H^+ and H_2^+) to secondary ion currents of niobium on time of the ion etching. Values of ordinates presented in a smoothed form.

3.3. Third Series of Experiments

The third series of SIMS measurements was carried out on AR, EP, and MEP samples taking into account the same mass parameters of secondary ions alike those of the second series. The positive secondary ions of four masses: 1, 2, 16, and 93 were studied. Ion mass etching with the beam of 5 keV Ar^+ was used. In view of reducing the edge effects during ion etching, the etching area was enlarged. For the studies, the etching area was 3.5 mm \times 3.5 mm. Etching time of the process was 3600 s resulting in the crater of depth equaling to about 65 nm. Herewith, the ion-etching rate of niobium was 0.016 nm \cdot s $^{-1}$.

SIMS studies with the craters $3.5\text{ mm} \times 3.5\text{ mm}$ were carried out to register positive secondary ions. In Figure 8, the holder with three niobium samples, AR, EP, and MEP, and slightly visible craters are shown (see one of them indicated by an arrow). The study results of this series are displayed in Figure 9.

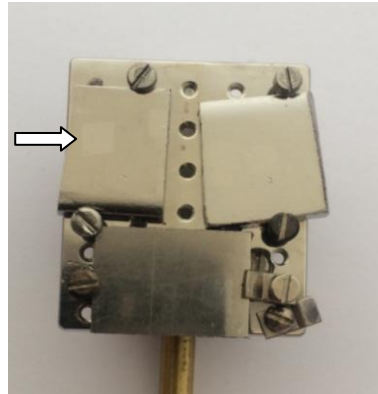


Figure 8. Holder with three Nb samples fixed onto it: EP—up on the left side, and MEP—up on the right side, and AR—down below. Well visible crater $3.5\text{ mm} \times 3.5\text{ mm}$, as marked by arrow, appears on EP niobium sample.

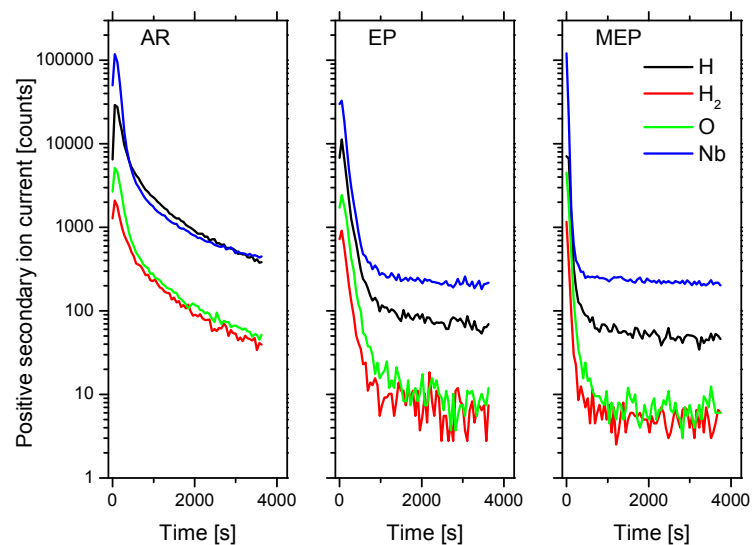


Figure 9. Primary results of SIMS depth profile analysis. Presented are values of secondary ions currents dependent on etching time using beam of 5 keV. The area of surface ion etching: $3.5\text{ mm} \times 3.5\text{ mm}$, the area of analysis: $1.35\text{ mm} \times 1.35\text{ mm}$.

Results obtained in this series (Figure 9) show that the number of the H^+ ions emission is the lowest on MEP sample. These results are somewhat different from those obtained on the sample with craters $1\text{ mm} \times 1\text{ mm}$, and much different from those with craters $2\text{ mm} \times 2\text{ mm}$. The reasons lie probably in edge effects and other selection in measurement parameters of the H^+ ions currents during $2\text{ mm} \times 2\text{ mm}$ craters' analysis. Another interesting observation here is a sharp drop in oxygen content on the MEP sample. Here also thickness of the oxide film is much lesser on MEP sample in comparison with that one measured on EP sample.

One may easily notice that the runs of secondary ions currents on niobium samples (Figure 8) are clearly different in three samples (AR, EP, MEP). To check and confirm these results, another additional measurements were carried out on two niobium samples, EP and MEP, taking etching time of 600 s. Results of these measurements are given in Figures 10 and 11.

In Figure 10 the smoothed results (B-Spline) in the range of 900 s time of ion etching are given, and for two of the samples, EP and MEP, results of rough SIMS profile analyses are displayed (Figure 11). The same analysis parameters were used: scattering area of 3.5 mm × 3.5 mm, and the analysis area of 1.35 mm × 1.35 mm.

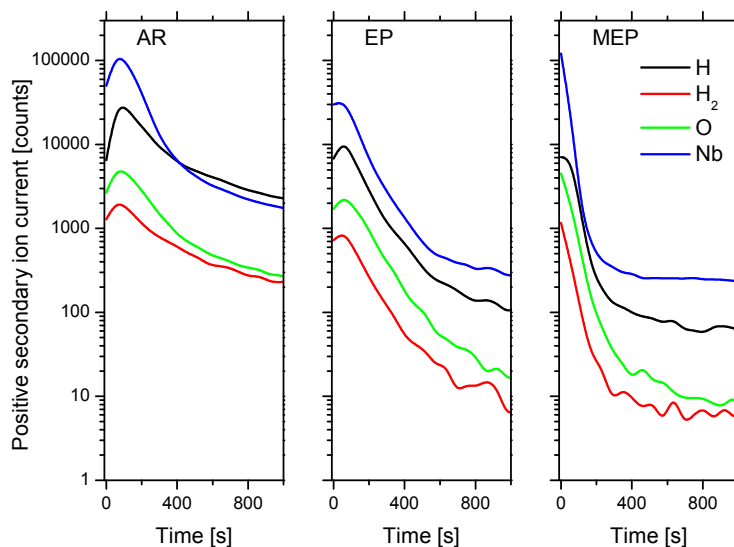


Figure 10. Results of rough SIMS depth analyses in the range of 900 s time of ion etching. Smoothed data: B-Spline.

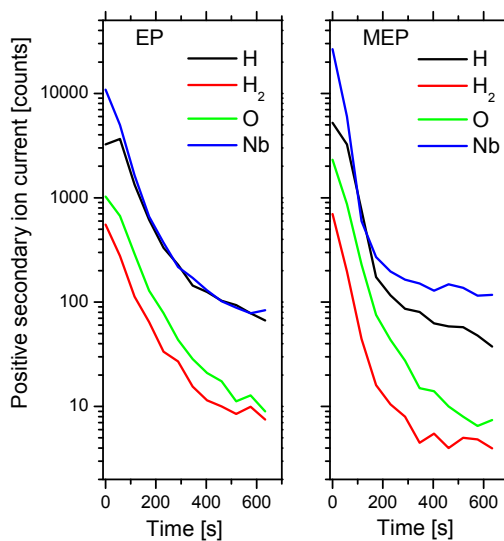


Figure 11. Results of rough SIMS depth analyses in the range of 600 s time of ion etching. Two additional measurements of EP and MEP samples are shown. The same analysis parameters used: scattering area: 3.5 mm × 3.5 mm, the analysis area: 1.35 mm × 1.35 mm.

Results presented in Figure 11 appear to be very similar to those displayed in Figures 9 and 10. Ion H^+ currents drop is falling faster on MEP sample in comparison with that one of EP sample.

To study the distribution of hydrogen concentration in the near-surface layers, another approach was done, presenting comparison of H^+ and H_2^+ ions emission with the niobium Nb^+ ions currents emission. In Figure 12, change in the ratio of hydrogen positive secondary ions (H^+ and H_2^+) currents to the niobium secondary ions currents vs. the ion etching time is given. Here the etching time of 3600 s corresponds with depth of the niobium etched layer equaling to about 70 nm.

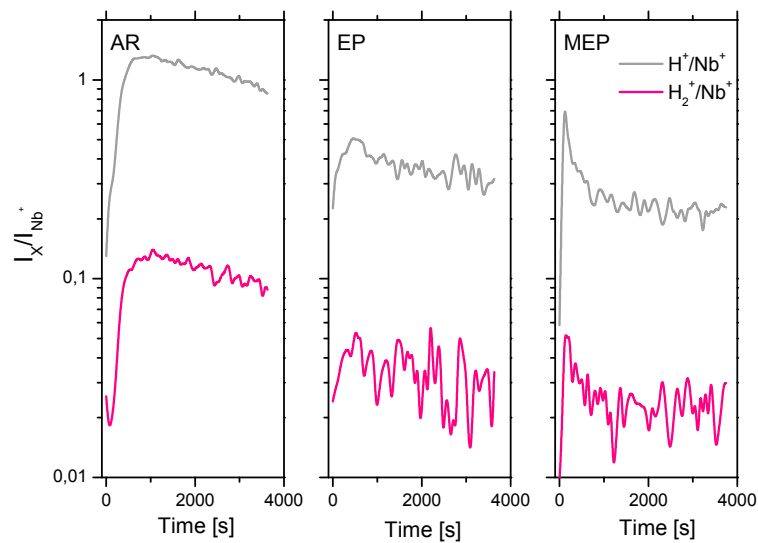


Figure 12. Change in the ratio of hydrogen positive secondary ions (H^+ and H_2^+) currents to the niobium secondary ions currents vs. the ion etching time. Etching time 3600 s corresponds with depth of the niobium etched layer equaling to about 70 nm.

In Figure 13, there are results presenting the positive secondary ion currents dependent on the depth of penetration in the range from top surface down to 17 nm in-depth. A constant rate of etching was assumed. In Figure 13a, there are rough data presented, and in Figure 13b—smoothed plots by B-Spline are given.

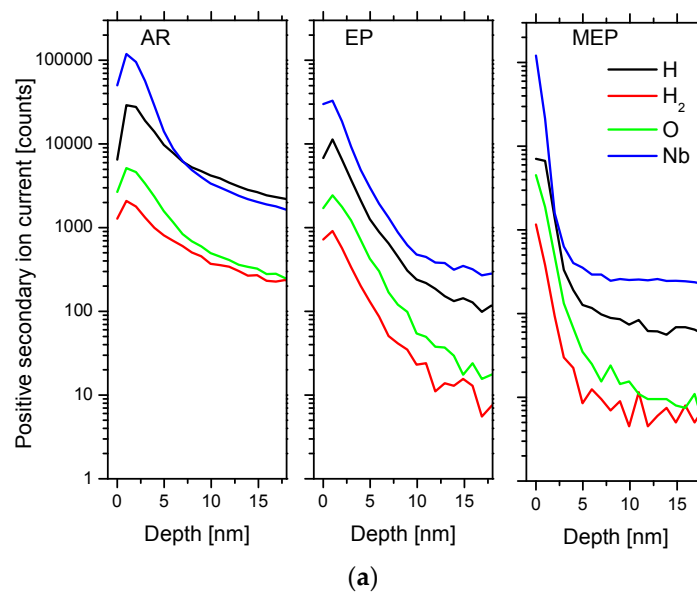


Figure 13. Cont.

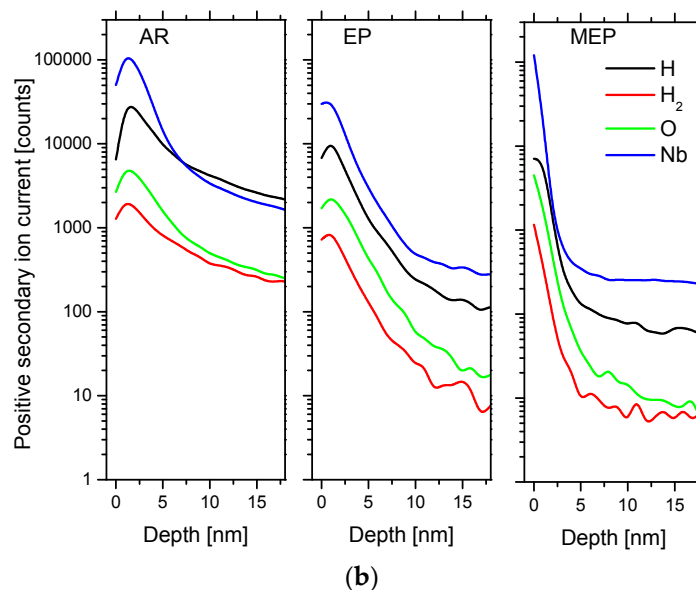


Figure 13. Results of secondary ion currents values dependent on the depth of ion etching in the range from top surface down to 17 nm in-depth: (a) rough data, and (b) smoothed plots: B-Spline.

One can clearly notice that the thinnest oxide layer was obtained on sample MEP, after magnetoelectropolishing. Also the hydrogen ion current emission decreases sharply during etching of this layer on the sample MEP. Its thickness is only about 1–2 nm. On EP niobium sample this oxide layer is about 3 nm thick, and on AR sample—about 4 nm. One should notice here that they are estimated values only, obtained basing on the drop of H^+ secondary ion currents, with the simultaneous assumption that the rate of etching of this oxide layer is the same as that one in case of etching pure/metallic niobium.

Changes of rates of hydrogen to niobium ions (H^+/Nb^+ and H_2^+/Nb^+) currents indicate that the highest possible content of hydrogen is in sample AR—after cold-rolling, some lower in EP sample, and the least one—in MEP sample (Figure 14). In Figure 15, separated results for H^+ and H_2^+ ions, related to AR, EP, and MEP niobium samples, are presented.

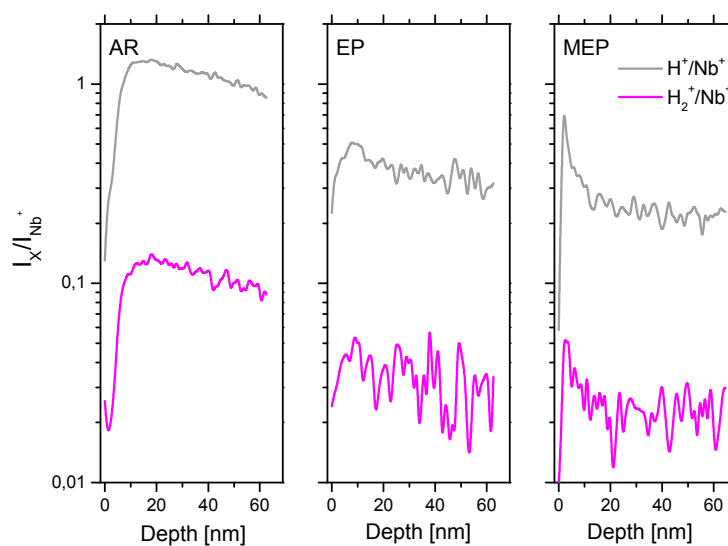


Figure 14. Dependence of rates of hydrogen positive secondary ions (H^+ and H_2^+) currents to the secondary niobium ion currents on the depth of ion etching.

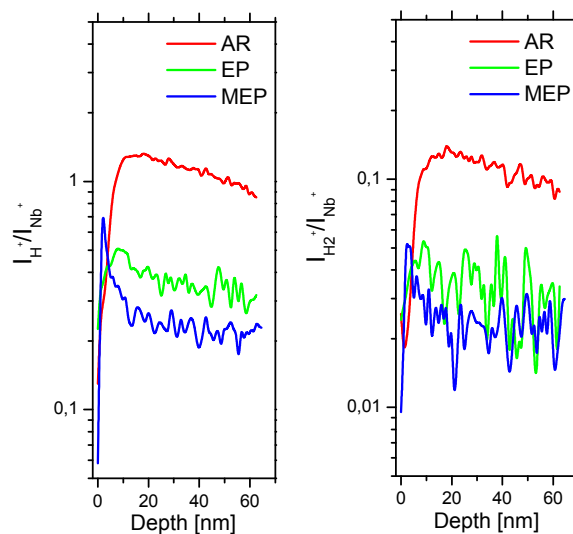


Figure 15. Dependence of rates of hydrogen positive secondary ions (H^+ and H_2^+) currents to the secondary niobium ion currents on the depth of ion etching. Separated results for H^+ and H_2^+ ions are displayed.

Figure 16 is provided to illustrate, how the hydrogen ion emission is changing during SIMS etching of near-surface layer of three investigated Nb samples: AR, EP, and MEP. By assuming that the thickness of oxide layer may be assessed taking into consideration half-value of the falling current, the estimated thicknesses of the surface layers' niobium samples are as follows: AR—about 4 nm, EP—3 nm, and MEP—about 1.5 nm.

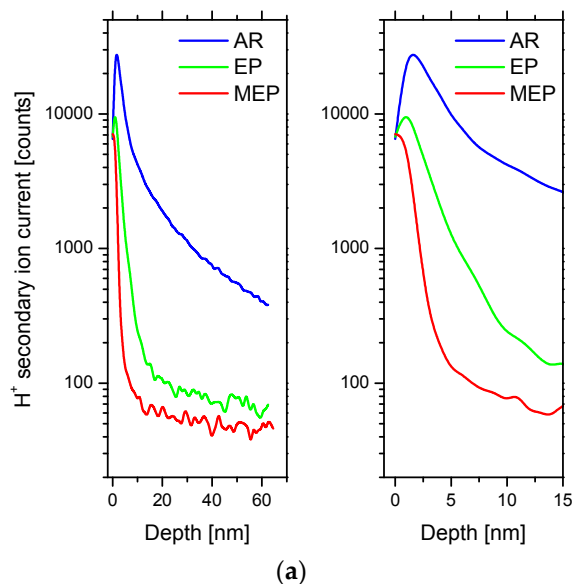


Figure 16. *Cont.*

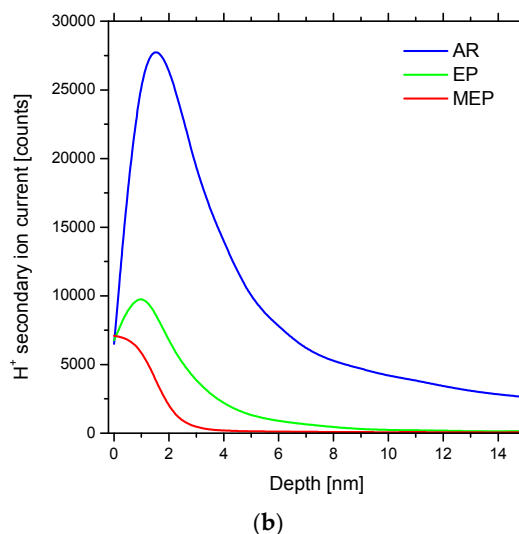


Figure 16. Comparison of plots obtained for H^+ ion currents against the depth of ion etching: (a) range of 0 to 65 nm, and (b) results covering range of etching from 0 down to 15 nm. In Figure 16b—smoothed data (B-Spline) are presented.

4. Discussion

Quantitative SIMS analysis of hydrogen in materials is very difficult, as there are number of factors influencing the measurement result [46]. The main problem is contamination of the sample's surface with hydrogen (mainly water). An additional problem is in situ contamination in the vacuum chamber of the mass spectrometer. The purpose of this paper is not to describe absolute hydrogen concentration but to compare the hydrogen content within the surface layers of the tested samples. Thus, all the samples after the electropolishing process were subjected to the same careful storage procedure. In order to limit “in situ” contamination, SIMS measurements were done in 3×10^{-8} Pa base vacuum.

The studies on hydrogenation level of electrochemically polished niobium samples, by using secondary ion mass spectrometry (SIMS), are presented in the paper. The program of the study covered three kinds of niobium samples: (1) AR—as received, material after cold-rolling, without any surface treatment, (2) EP—Nb samples after a standard electropolishing, and (3) MEP—samples after magneto-electropolishing. Time of this SIMS analysis was 6000 s.

The first series of our SIMS studies of niobium appeared to be charged with strong edge effects, and with these presenting rather unreliable results. One could find very similar level of H^+ ion emission in both EP and MEP electrochemically treated samples. The assumed depth of penetration in the SIMS studies could suggest there is no essential difference in hydrogen concentration of EP and MEP samples. Also the character of courses of H^+ and H_2^+ ion currents is very similar, but the intensity of H_2^+ ion currents is ten times less than that of H^+ ion currents.

Niobium samples after EP and MEP treatments were applied to the second series of SIMS measurements. In this series, a lesser area of ionic etching was applied, equaling $1 \text{ mm} \times 1 \text{ mm}$, with the area of SIMS analysis reduced down to $0.4 \text{ mm} \times 0.4 \text{ mm}$. The time of the SIMS analysis was assumed to be 5000 s. The results obtained in this series show that investigated positive secondary currents are very similar on both samples, EP and MEP (Figures 5 and 6). However, the dependence of ratios of secondary ions currents for positive hydrogen (H^+ and H_2^+) to the secondary ion currents of niobium on time of the ion etching reveals a slight difference between EP and MEP niobium samples (Figure 7). Smoothed forms of the ordinates values presented by dots in Figure 7 indicate the reduced values regarding MEP samples, which can be easily noticed.

This behavior of ion currents prompted us to carry out the third series of SIMS experiments paying a special attention to the edge effects. With this series of SIMS measurements, all niobium samples—AR,

EP, and MEP—were taken into consideration, with the mass parameters of secondary ions same as those of the second series. The etching area in this series was $3.5 \text{ mm} \times 3.5 \text{ mm}$, assuming 3600 s as the etching time of the process. The crater of depth of about 65 nm, and the ion etching rate of niobium equaling $0.016 \text{ nm}\cdot\text{s}^{-1}$ resulted in getting clarification of the data obtained and much more meaningful effects of the studies.

In Figure 17, an illustration of estimated depth to which the hydrogen content is expected has been provided, with the highest concentration measured on AR sample. The electrochemical treatments with the EP and MEP processes result both in lowering the hydrogenation and a significant shift in the beginning of SIMS measurement in all plots presented above.

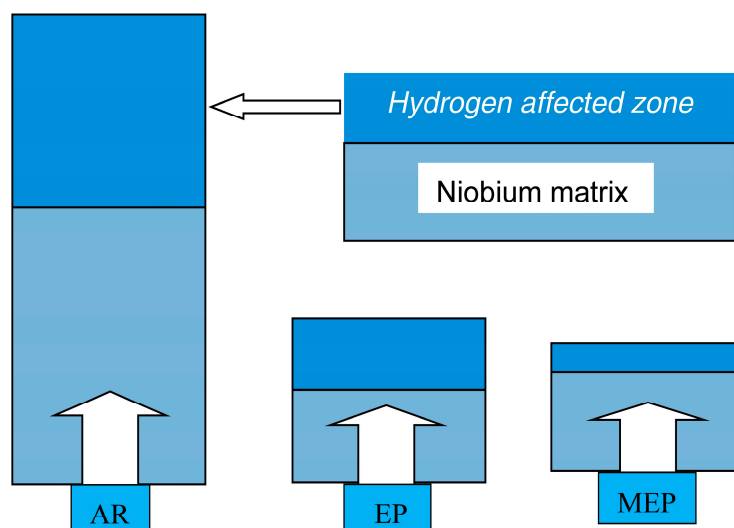


Figure 17. Comparable zone affected by hydrogen in Nb sample: AR—as received, EP—after electropolishing, MEP—after magnetoelectropolishing.

By limiting the edge effects and other selections in measurement parameters of the H^+ ions currents for this analysis, the level of the H^+ ions emission appeared to be the lowest on MEP sample, as expected from our earlier studies (see refs. of the study on 316L SS [44] and Ti [45]). One more interesting phenomenon noticed here was a sharp decrease in oxygen content in the surface film of the MEP sample. All herewith presented results show that the thickness of the oxide film is much lower on the MEP niobium sample in comparison with that one found on EP sample.

The next two niobium samples, EP and MEP, were investigated by assuming etching time of 3600 s and the SIMS measurements results are given in Figure 12. They allowed us to estimate thicknesses of surface oxide film on the niobium samples to be of the magnitudes as follows: AR—about 4 nm, EP—3 nm, and MEP—about 1.5 nm.

5. Conclusions

The studies carried out on niobium allowed us to formulate the following conclusions:

- Niobium (AR—as received) may be electropolished (EP) and/or magnetoelectropolished (MEP) using compounded electrolyte consisting of mixture of 70% methanesulfonic acid with 49% hydrofluoric acid by volume in a 3:1 ratio
- SIMS measurements have shown that the lowest hydrogenation level was achieved on MEP niobium samples in comparison with that one measured before (AR samples) and after other electrochemical treatments (EP samples)
- The estimated thicknesses of the surface layers' niobium samples are as follows: AR—about 4 nm, EP—3 nm, and MEP—about 1.5 nm

The MEP process in new electrolyte is advised for surface finishing of niobium with the sped-up metal removal in-depth on request.

Author Contributions: Tadeusz Hryniewicz and Ryszard Rokicki conceived and designed the experiments; Piotr Konarski and Ryszard Rokicki performed the experiments; Tadeusz Hryniewicz and Piotr Konarski analyzed the data; Tadeusz Hryniewicz, Piotr Konarski, and Ryszard Rokicki contributed reagents, materials, analysis tools; Tadeusz Hryniewicz and Piotr Konarski wrote the paper.

Conflicts of Interest: The authors declare no conflict of interest.

References

1. Pienaar, A.D.; Wagener, J.B.; Crouse, P.L. Niobium and tantalum separation by gas-phase fluorination. *Int. J. Miner. Proc.* **2012**, *7*, 114–117. [[CrossRef](#)]
2. Buch, A. Pure metals properties. In *A Scientific-Technical Handbook*, 1st ed.; Buch, A., Ed.; ASM International and Freund Publishing House Ltd.: Materials Park, OH, USA, 1999; p. 360.
3. Ahn, Y.S.; Kim, H.D.; Byun, T.S.; Oh, Y.J.; Kim, G.M.; Hong, J.H. Application of intercritical heat treatment to improve toughness of SA508 Cl.3 reactor pressure vessel steel. *Nucl. Eng. Des.* **1999**, *194*, 161–177. [[CrossRef](#)]
4. Lee, K.H.; Kim, M.C.; Yang, W.J.; Lee, B.S. Evaluation of microstructural parameters controlling cleavage fracture toughness in Mn-Mo-Ni low alloy steels. *Mater. Sci. Eng. A* **2013**, *565*, 158–164. [[CrossRef](#)]
5. Niobium's Use in Nuclear Reactor. Available online: <http://www.studymode.com/essays/Niobium-s-Use-Nuclear-Reactors-64970998.html> (accessed on 10 May 2017).
6. Romanenko, A.; Barkov, F.; Cooley, L.D.; Grassellino, A. Proximity breakdown of hydrides in superconducting niobium cavities. *Supercond. Sci. Technol.* **2013**, *26*. [[CrossRef](#)]
7. Wu, G.; Ge, M.; Kneisel, P.; Zhao, K.; Cooley, L.D.; Ozelis, J.; Sergatskov, D.; Cooper, C. *Investigations of Surface Quality and SRF Cavity Performance*; 2LP1C-02, FERMILAB-CONF-10-430-TD; 2010; pp. 1–4. Available online: <http://lss.fnal.gov/archive/2010/conf/fermilab-conf-10-430-td.pdf> (accessed on 7 April 2017).
8. Nikulina, V. Metal materials for the elements of nuclear reactors: Zirconium-niobium alloys for core elements of pressurized water reactors. *Met. Sci. Heat Treat.* **2003**, *45*, 287–292. [[CrossRef](#)]
9. Ramanjaneyulu, P.S.; Sayi, Y.S.; Ramakumar, K.L. Determination of boron in zirconium-niobium alloys by spectrophotometry. *Indian J. Chem. Technol.* **2010**, *17*, 468–470.
10. Morgan, A.V.; Romanenko, A.; Windsor, A. Surface studies of contaminants generated during electropolishing. WEPMS010. In Proceedings of the PAC07, 22nd Conference on Particle accelerator, Albuquerque, NM, USA, 25–29 June 2007; pp. 2346–2348. Available online: <http://accelconf.web.cern.ch/Accelconf/p07/PAPERS/WEPMS010.PDF> (accessed on 12 April 2017).
11. Saito, K. Surface Smoothness for High Gradient Niobium SC RF Cavities. 2003. Available online: <http://srf.desy.de/fap/paper/ThP15.pdf> (accessed on 12 April 2017).
12. Tegtart, W.J.M. *The Electrolytic and Chemical Polishing of Metals for Research and Industry*; Pergamon Press: London, UK, 1956.
13. Diepers, H.; Schmidt, O.; Martens, H.; Sun, F.S. A new method of electropolishing niobium. *Phys. Lett. A* **1971**, *37*, 139–140. [[CrossRef](#)]
14. Hryniewicz, T.; Hryniewicz, Z. On the Solution of Equation of Diffusion in Electropolishing. *J. Electrochem. Soc.* **1989**, *136*, 3767–3769. [[CrossRef](#)]
15. Hryniewicz, T. Concept of Microsmoothing in the Electropolishing Process. *Surf. Coat. Technol.* **1994**, *64*, 75–80. [[CrossRef](#)]
16. Rokicki, R.; Hryniewicz, T. Enhanced oxidation-dissolution theory of electropolishing. *Trans. Inst. Met. Finish.* **2012**, *90*, 188–196. [[CrossRef](#)]
17. Rokosz, K.; Simon, F.; Hryniewicz, T.; Rządkiwicz, S. Comparative XPS analysis of passive layers composition formed on duplex 2205 SS after standard and high-current density electropolishing. *Tehnicki Vjesnik-Teh. Gaz.* **2016**, *23*, 731–735. [[CrossRef](#)]
18. Hryniewicz, T.; Rokosz, K.; Rokicki, R.; Prima, F. Nanoindentation and XPS Studies of Titanium TNZ Alloy after Electrochemical Polishing in a Magnetic Field. *Materials* **2015**, *8*, 205–215. [[CrossRef](#)] [[PubMed](#)]
19. Rokicki, R.; Hryniewicz, T.; Pulletikurthi, C.; Rokosz, K.; Munroe, N. Towards a better corrosion resistance and biocompatibility improvement of nitinol medical devices. *J. Mater. Eng. Perform.* **2015**, *24*, 1634–1640. [[CrossRef](#)]

20. Rokosz, K.; Lahtinen, J.; Hryniewicz, T.; Rzadkiewicz, S. XPS depth profiling analysis of passive surface layers formed on austenitic AISI 304L and AISI 316L SS after high-current-density electropolishing. *Surf. Coat. Technol.* **2015**, *276*, 516–520. [[CrossRef](#)]
21. Rokosz, K.; Hryniewicz, T.; Rzadkiewicz, S.; Raaen, S. High-current-density electropolishing (HDEP) of AISI 316L SS (EN 1.4404) stainless steel. *Tehnicki Vjesnik-Teh. Gaz.* **2015**, *22*, 415. [[CrossRef](#)]
22. Rokosz, K.; Simon, F.; Hryniewicz, T.; Rzadkiewicz, S. Comparative XPS analysis of passive layers formed on AISI 304L SS after standard and very-high-current density electropolishing. *Surf. Interface Anal.* **2015**, *47*, 87. [[CrossRef](#)]
23. Hryniewicz, T.; Rokosz, K.; Zschommler Sandim, H.R. SEM/EDX and XPS studies of niobium after electropolishing. *Appl. Surf. Sci.* **2012**, *263*, 357–361. [[CrossRef](#)]
24. Rokicki, R.; Hryniewicz, T.; Konarski, P.; Rokosz, K. The alternative, novel technology for improvement of surface finish of SRF niobium cavities. *World Sci. News* **2017**, *74*, 152–163.
25. Rokosz, K.; Hryniewicz, T.; Matysek, D.; Dudek, L.; Valiček, J.; Harničarova, M.; Kušnerova, M.; Zschommler Sandim, H.R. SEM and EDS analysis of niobium surface after plasma electrolytic oxidation in concentrated phosphoric acid within copper nitrate. In Proceedings of the 25th Anniversary International Conference on Metallurgy and Materials (METAL 2016), Brno, Czech Republic, 25–27 May 2016; pp. 1157–1162.
26. Rokosz, K.; Hryniewicz, T. Comparative SEM and EDX analysis of surface coatings created on niobium and titanium alloys after plasma electrolytic oxidation (PEO). *Tehnicki Vjesnik-Teh. Gaz.* **2017**, *24*, 465–472.
27. Hryniewicz, T.; Rokosz, K.; Rokicki, R. Magneto-electropolishing process improves characteristic of finished metal surface. *Met. Finish.* **2006**, *104*, 26–31. [[CrossRef](#)]
28. Hryniewicz, T.; Rokicki, R.; Rokosz, K. Magneto-electropolishing for metal surface modification. *Trans. Inst. Metal Finish.* **2007**, *85*, 325–332. [[CrossRef](#)]
29. Rokicki, R.; Hryniewicz, T. Nitinol™ surface finishing by magneto-electropolishing. *Trans. Inst. Met. Finish.* **2008**, *86*, 280–285. [[CrossRef](#)]
30. Hryniewicz, T.; Rokosz, K. Analysis of XPS results of AISI 316L SS electropolished and magneto-electropolished at varying conditions. *Surf. Coat. Technol.* **2010**, *204*, 2583–2592. [[CrossRef](#)]
31. Rokosz, K. *Electrochemical Polishing in the Magnetic Field*; Koszalin University of Technology Publishing House: Koszalin, Poland, 2012. (In Polish)
32. Hryniewicz, T.; Rokosz, K.; Valiček, J.; Rokicki, R. Effect of magneto-electropolishing on nanohardness and Young modulus of titanium biomaterial. *Mat. Lett.* **2012**, *83*, 69–72. [[CrossRef](#)]
33. Hryniewicz, T.; Rokosz, K.; Rokicki, R. Magnetic fields for electropolishing improvement: Materials and systems. *Int. Lett. Chem. Phys. Astron.* **2014**, *4*, 98–108. [[CrossRef](#)]
34. Rokosz, K.; Hryniewicz, T. XPS Analysis of nanolayers obtained on AISI 316L SS after Magneto-electropolishing. *World Sci. News* **2016**, *37*, 232–248.
35. Pundt, A.; Kirchheim, R. Hydrogen in metals: Microstructural aspects. *Annu. Rev. Mater. Res.* **2006**, *36*, 555–608. [[CrossRef](#)]
36. Konarski, P.; Mierzejewska, A. B₄C/Mo/Si and Ta₂O₅/Ta nanostructures analysed by ultra-low energy argon ion beams. *Appl. Surf. Sci.* **2003**, *203–204*, 354–358. [[CrossRef](#)]
37. Magee, C.W.; Botnick, E.M. Hydrogen depth profiling using SIMS—Problems and their solutions. *J. Vac. Sci. Technol.* **1981**, *19*, 47. [[CrossRef](#)]
38. Clark, G.J.; White, C.W.; Allred, D.D.; Appleton, B.R.; Magee, C.W.; Carlson, D.E. The use of nuclear reactions and SIMS for quantitative depth profiling of hydrogen in amorphous silicon. *Appl. Phys. Lett.* **1977**, *31*, 582. [[CrossRef](#)]
39. Wittmaack, K. Background formation in SIMS analysis of hydrogen, carbon, nitrogen and oxygen in silicon. *Nucl. Instrum. Meth. Phys. Res.* **1983**, *218*, 327–332. [[CrossRef](#)]
40. Hultquist, G.; Graham, M.J.; Kodra, O.; Moisa, S.; Liu, R.; Bexell, U.; Smialek, J.L. Corrosion of copper in distilled water without O₂ and the detection of produced hydrogen. *Corros. Sci.* **2015**, *95*, 162–167. [[CrossRef](#)]
41. Toda, T.; Wang, D.; Jiang, J.; Hung, M.P.; Furuta, M. Quantitative analysis of the effect of hydrogen diffusion from silicon oxide etch-stopper layer into amorphous In-Ga-Zn-O on thin film transistor. *IEEE Trans. Electron Dev.* **2014**, *61*, 3762–3767. [[CrossRef](#)]
42. Othmane, G.; Hull, S.; Fayek, M.; Rouxel, O.; Geagea, M.L.; Kyser, T.K. Hydrogen and copper isotope analysis of turquoise by SIMS: Calibration and matrix effects. *Chem. Geol.* **2015**, *395*, 41–49. [[CrossRef](#)]

43. Makówka, M.; Pawlak, W.; Konarski, P.; Wendler, B. Hydrogen content influence on tribological properties of nc-WC/aC:H coatings. *Diam. Relat. Mater.* **2016**, *67*, 16–25. [[CrossRef](#)]
44. Hryniewicz, T.; Konarski, P.; Rokicki, R.; Valiček, J. SIMS studies of titanium biomaterial hydrogenation after magnetoelectropolishing. *Surf. Coat. Technol.* **2012**, *206*, 4027–4031. [[CrossRef](#)]
45. Hryniewicz, T.; Konarski, P.; Rokicki, R.; Valiček, J. SIMS analysis of hydrogen content in near surface layers of aisi 316l ss after electrolytic polishing under different conditions. *Surf. Coat. Technol.* **2011**, *205*, 4228–4236. [[CrossRef](#)]
46. Ludwig, T.; Stalder, R. A new method to eliminate the influence of in situ contamination in SIMS analysis of hydrogen. *J. Anal. At. Spectrom.* **2007**, *22*, 1415–1419. [[CrossRef](#)]



© 2017 by the authors. Licensee MDPI, Basel, Switzerland. This article is an open access article distributed under the terms and conditions of the Creative Commons Attribution (CC BY) license (<http://creativecommons.org/licenses/by/4.0/>).